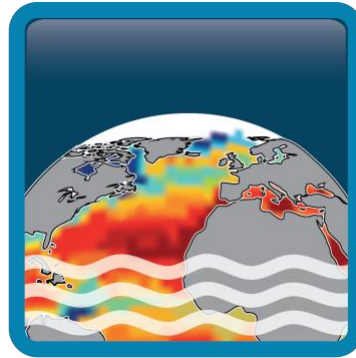


# Climate Change Initiative+ (CCI+) Phase 1

## Sea Surface Salinity



### End-to-End ECV Uncertainty Budget (E3UB)

Customer: ESA

Ref.: ESA-CCI-PRGM-EOPS-SW-17-0032

Version: v3.1

Ref. internal: AO/1-9041/17/I-NB\_v3r0

Revision Date: 13/09/2021

Filename: SSS\_cci-D2.3-E3UB-v3.0

Deliverable code: D2.3





## Signatures

Author	Jean Luc Vergely		13-09-2021
Reviewed by	Jacqueline Boutin (Science Leader)		
Approved By	Jacqueline Boutin (Science Leader)		13-09-2021
	Nicolas Reul (Science Leader)		
	Rafael Catany (Project Manager)		13-09-2021
Accepted by	Susanne Mecklenburg (Technical Officer) ESA		

Diffusion List
Sea Surface Salinity Team Members
ESA (Susanne Mecklenburg, Paolo Cipollini, Roberto Sabia)



## Amendment Record Sheet

DATE / ISSUE	DESCRIPTION	SECTION / PAGE
15-07-2019 / v1.0	Delivery to ESA	New document
21-10-2019 / v1.1	Update reference document documents section	Section 1.3.2 / page 14
	Implemented description of the sensors mounted in each satellite	Section 2 / page 21 – 22
	Added overview about PIMEP	Section 4.4.2 / page 31
	Added definition PCTVAR	Section 5.3.1 / page 63
	Improved Figure 33. Now all markers are visible as described in figure caption.	Section 5.3.2 / page 65
19/12/2019 / v1.2	Edited description about PIMEP	Section 4.4.2 / page 31
19/12/2019 / v1.2	Added band width of Aquarius satellite is 25 MHz	Section 2.4 / page 22
19/12/2019 / v1.2	Added clarification text about Figure 32, stating that further analyses is needed and it will be provided in next version of the document.	Section 5.2.2 / page 60
19/12/2019 / v1.2	Edited caption Figure 34. Now the caption read “2016-2018” as seen in the main text too.	Section 5.3.2 / page 63
08-07-2020 / v2.1	Document update for delivery MS#04 to ESA	Version 2.1 of the document
10-11-2020 / v2.2	Implement ESA’s feedback (minor changes)	N/A
13-09-2021 / v3.1 (this document)	Phase 1 final version	All



## Table of Contents

<b>1</b>	<b>Introduction .....</b>	<b>10</b>
1.1	Scope of this document .....	10
1.2	Structure of the document .....	10
1.3	References .....	10
1.3.1	Applicable Documents .....	10
1.3.2	Reference Documents .....	11
1.4	Acronyms .....	13
<b>2</b>	<b>Sensor main characteristics.....</b>	<b>19</b>
2.1	Introduction.....	19
2.2	SMOS.....	19
2.3	SMAP.....	19
2.4	Aquarius .....	20
<b>3</b>	<b>L1 uncertainty characterization.....</b>	<b>21</b>
3.1	Introduction.....	21
3.2	SMOS sensor.....	21
3.3	SMAP and Aquarius sensors .....	22
3.4	RFI filtering .....	22
<b>4</b>	<b>L2OS uncertainty characterization .....</b>	<b>24</b>
4.1	Introduction.....	24
4.2	Methods .....	24
4.2.1	Random uncertainty estimation.....	24
4.2.2	Systematic uncertainty estimation.....	26
4.3	Spatial sampling .....	28
4.4	Uncertainty estimation methods applied to SMOS, SMAP and Aquarius. ....	29
4.4.1	Introduction.....	29
4.4.2	PI-MEP (from <a href="https://www.smos-pimep.org/overview.html">https://www.smos-pimep.org/overview.html</a> ).....	29
4.4.3	External data.....	30
4.4.4	Data analysis.....	30
<b>5</b>	<b>L3 and L4 uncertainty budget.....</b>	<b>44</b>
<b>6</b>	<b>Conclusions and way forward .....</b>	<b>45</b>

## List of figures

Figure 1: EASE grid (undersampling of a factor of 10). -----	29
Figure 2: histogram of the new random variable X (reduced centered SSS) after applying a coastal correction. Top: pixels near the coast (dcoast<400 km); bottom: pixels in the open ocean. March 2012. -----	34
Figure 3: uncertainty factor according to the distance to the coast.-----	35
Figure 4: Mask applied to SMOS data for latitudinal bias computation. -----	36
Figure 5: example of latitudinal correction for the month of January. The x axis corresponds to the ascending dwell lines and the descending dwell lines, the y axis corresponds to the latitude. Such a diagram is available for each month of the year (12-month periodicity). -----	36
Figure 6: example of SMOS bias (relative +absolute) calculated for xswath=363 km. Top: ascending orbits; bottom, descending orbits.-----	37
Figure 7: example of SMOS bias (relative +absolute) calculated for xswath=13km. Top: ascending orbits; bottom, descending orbits. -----	37
Figure 8: SSS SMAP uncertainty obtained by comparing aft and fore acquisitions. -----	39
Figure 9: uncertainty factor according to the distance to the coast. SMAP. -----	39
Figure 10: SMAP bias (relative +absolute) calculated for aft acquisitions. Top: ascending orbits; bottom, descending orbits. -----	40
Figure 11: SMAP bias (relative +absolute) calculated for fore acquisitions. Top: ascending orbits; bottom, descending orbits. -----	40
Figure 12: SSS Aquarius uncertainty obtained by comparing 7 day acquisitions. -----	42
Figure 13: uncertainty factor according to the distance to the coast. Aquarius. -----	42
Figure 14: Hovmöller diagram of Aquarius latitudinal biases (SSS Aquarius - SSS SMAP). Top: ascending orbits. Bottom: descending orbits.-----	43
Figure 15: Aquarius bias (relative +absolute). Top: ascending orbits; bottom, descending orbits. -----	43

## List of tables

No table of figures entries found.



# 1 Introduction

## 1.1 Scope of this document

---

This document holds the End-to-End ECV Uncertainty Budget (E3UB) prepared by CCI+ Salinity team, as part of the activities included in the [WP240] of the Proposal (Task 2 from SoW ref. ESA-CCI-PRGM-EOPS-SW-17-0032).

SSS measurements are available from three L-Band radiometer satellite missions, SMOS, Aquarius and SMAP, each with very different instrument features leading to particular measurement characteristics. The Climate Change Initiative Salinity project (CCI+SSS) aimed to produce SSS Climate Data Record (CDR) to include satellite measurements together with well documented uncertainties. To establish a homogeneous CDR, instrumental differences are carefully controlled by analysing SSS discrepancies, then adjusted based on deepened analysis of the satellite measurements themselves together with independent reference data. This document describes the basis for the uncertainties characterizations.

## 1.2 Structure of the document

---

The E3UB is structured as follows:

This document is composed of 4 major sections:

- ✓ Section 2: Sensor main characteristics
- ✓ Section 3: L1 uncertainty characterization
- ✓ Section 4: L2 uncertainty characterization
- ✓ Section 5: L3 and L4 uncertainty budget

L2/L3/L4 data sets will be provided each year and are described in the SRD.

This is the third version of the E3UB document addressing Year 3 activity.

## 1.3 References

---

### 1.3.1 Applicable Documents

ID	Document	Reference
AD01	CCI+ Statement of Work	SoW
AD02	Product User Guide (PUG)	SSS_cci-D4.3-PUG-v3.0
AD03	User Requirement Document (URD)	SSS_cci-D1.1-URD-v2.0
AD04	Product Specification Document (PSD)	SSS_cci-D1.2-PSD-v2.0



ID	Document	Reference
<b>AD05</b>	Algorithm Theoretical Baseline Document	SSS_cci-D2.3-ATBD_L3_L4-i1r0_v1.1
<b>AD06</b>	End-to-End ECV Uncertainty Budget (E3UB), version 1	SSS_cci-D2.3-E3UB_v1.2
<b>AD07</b>	Algorithm Theoretical Baseline Document, version 2	SSS_cci-D2.3-ATBD_L3_L4-i1r0_v2.0
<b>AD08</b>	End-to-End ECV Uncertainty Budget (E3UB), version 2	SSS_cci-D2.3-ATBD_L3_L4-i1r0_v2.2
<b>AD09</b>	Algorithm Theoretical Baseline Document, version 3	SSS_cci-D2.3-ATBD_L3_L4-i1r0_v3.0

### 1.3.2 Reference Documents

ID	Document	Reference
<b>RD01</b>	Boutin, J., N. Martin, N. Kolodziejczyk, and G. Reverdin (2016a), Interannual anomalies of SMOS sea surface salinity, <i>Remote Sensing of Environment</i> , doi:http://dx.doi.org/10.1016/j.rse.2016.02.053	
<b>RD02</b>	Kolodziejczyk, N., J. Boutin, J.-L. Vergely, S. Marchand, N. Martin, and G. Reverdin (2016), Mitigation of systematic errors in SMOS sea surface salinity, <i>Remote Sensing of Environment</i> , doi:http://dx.doi.org/10.1016/j.rse.2016.02.061.	
<b>RD03</b>	Evaluation of measurement data – Guide to the expression of uncertainty in measurement, JCGM 100:2008	
<b>RD04</b>	SMOS ATBD L2OS v3.13, 29 April 2016	SO-TN-ARG-GS-0007
<b>RD05</b>	AQ-014-PS-0017_Aquarius_L2toL3ATBD_DatasetVersion5.0 Liang Hong, Normal Kuring, Joel Gales and Fred Patt	
<b>RD06</b>	AQ-014-PS-0018_AquariusLevel2specification_DatasetVersion5.0 Fred Patt, Liang Hong	
<b>RD07</b>	SMAP_RemSSS_Release_V2.0	
<b>RD08</b>	Meissner, T. and F. J. Wentz, 2016: Remote Sensing Systems SMAP Ocean Surface Salinities [Level 2C, Level 3 Running 8-day, Level 3 Monthly], Version 2.0 validated release. Remote Sensing Systems, Santa Rosa, CA, USA. Available online at www.remss.com/missions/smap, doi: 10.5067/SMP20-2SOCS (L2C files).	
<b>RD09</b>	Boutin J., J.-L. Vergely, S. Marchand, F. D'Amico, A. Hasson, N. Kolodziejczyk, N. Reul, G. Reverdin, J. Vialard (2018), New SMOS Sea Surface Salinity with reduced systematic errors and improved variability, <i>Remote Sensing of Environment</i> , doi:http://dx.doi.org/10.1016/j.rse.2018.05.022	
<b>RD10</b>	Thomas Meissner + Frank Wentz Remote Sensing Systems, Santa Rosa, CA, RSS SMAP Salinity: Version 2 Validated Release. Algorithm Theoretical Basis Document (ATBD), September 13, 2016	RSS Technical Report 091316
<b>RD11</b>	Dinnat, E., D. Le Vine, J. Boutin, T. Meissner, and G. Lagerloef. 2019. "Remote Sensing of Sea Surface Salinity: Comparison of Satellite and In Situ Observations and Impact of Retrieval Parameters." <i>Remote Sensing</i> , <b>11 (7)</b> : 750	



**Climate Change Initiative+ (CCI+)  
Phase 1**

End-to-End ECV Uncertainty Budget

Ref.: ESA-CCI-PRGM-EOPS-SW-17-0032

Date: 13/09/2021

Version : v3.1

Page: 12 of 46

ID	Document	Reference
<b>RD12</b>	C. J. Merchant et al. (2017): Uncertainty information in climate data records from Earth observation, <i>Earth Syst. Sci. Data</i> , 9, 511-527	
<b>RD13</b>	Brodzik, M. J., B. Billingsley, T. Haran, B. Raup, and M. H. Savoie (2012), EASE-Grid 2.0: Incremental but Significant Improvements for Earth-Gridded Data Sets, <i>ISPRS International Journal of Geo-Information</i> , 1(1), 32-45.	
<b>RD14</b>	Le Vine, D. M., and P. de Mattheais (2014), Aquarius active/passive RFI environment at L-band, <i>IEEE Geosci. Remote Sens. Lett.</i> , 11(10), doi:10.1109/LGRS.2014.2307794.	



## 1.4 Acronyms

---

AD	Applicable Document
ADP	Algorithm Development Plan
AOPC	Atmospheric Observation Panel for Climate
AR	Assessment Report (of the IPCC)
AR6	IPCC Scientific Assessment Report 6
ATBD	Algorithm Theoretical Basis Document
Aquarius	NASA mission
C3S	Copernicus Climate Change Service
CAR	Climate Assessment Report
CCI	The ESA Climate Change Initiative (CCI) is formally known as the Global Monitoring for Essential Climate Variables (GMECV) element of the European Earth Watch programme
CCI+	Climate Change Initiative Extension (CCI+), is an extension of the CCI over the period 2017–2024
CDR	Climate Data Record
CEOS	Committee on Earth Observation Satellites
CFOSAT	Chinese French Oceanography Satellite
CGMS	Coordination Group for Meteorological Satellites
CLiC	World Climate Research Programme - Climate and Cryosphere Project
CLIVAR	WCRP Climate Variability and Predictability project
CMEMS	Copernicus Marine Environmental Monitoring Service
CMIP	Coupled Model Intercomparison Project
CMUG	Climate Modelling User Group
COP	Conference of the Parties
COWCLIP	Coordinated Ocean Wave Climate Project (of JCOMM)



CR	Cardinal Requirement
CRDP	Climate Research Data Package
CRG	Climate Research Group
CSCDA	Copernicus Space Component Data Access System
CSWG	Climate Science Working Group
DARD	Data Access Requirements Document
DEWG	Data Engineering Working Group
DOI	Digital Object Identifier
DPM	Detailed Processing Model
DTBT3	Database for Task 3
DUE	Data User Element
E3UB	End-to-End ECV Uncertainty Budget
EC	European Commission
ECMWF	European Centre for Medium Range Weather Forecasts
ECSAT	European Centre for Space Applications and Telecommunications
ECSS	European Cooperation for Space Standardization
ECV	Essential Climate Variable
EO	Earth Observation
EOV	Essential Ocean Variable (of the OOPC)
ESGF	Earth System Grid Federation
ESM	Earth System Model
EU	European Union
FCDR	Fundamental Climate Data Record
FIDUCEO	Fidelity and uncertainty in climate data records from Earth Observations
FOV	Field Of View



*Climate Change Initiative+ (CCI+)  
Phase 1*

End-to-End ECV Uncertainty Budget

Ref.: ESA-CCI-PRGM-EOPS-SW-17-0032

Date: 13/09/2021

Version : v3.1

Page: 15 of 46

FP7	EU Framework Programme 7
FRM	Fiducial Reference Measurements
GAIA-CLIM	Gap Analysis for Integrated Atmospheric ECV CLimate Monitoring
GEO	Group on Earth Observations
GCOS	Global Climate Observing System
GCW	Global Cryosphere Watch
GMECV	Global Monitoring of Essential Climate Variables - element of the European Earth Watch programme.
GNSS	Global Navigation Satellite System
GOOS	Global Ocean Observing System
H2020	Horizon 2020 programme
Hs	Significant Wave Height (see also SWH)
H-SAF	EUMETSAT's Hydrology Satellite Applications Facility
HDD	Hard disk
IOC	Intergovernmental Oceanographic commission (of UNESCO)
IODD	Input Output Data Definition
IP	Implementation Plan
IPCC	Intergovernmental Panel on Climate Change
ISAS	In Situ Analysis System (LOPS)
ISDB	in situ database (of Fiducial Reference Measurements and satellite measurements)
JAXA	Japan Aerospace Exploration Agency
JCOMM	Joint Commission on Oceanography and Marine Meteorology
KO	Kick-off
MOOC	Massive Open Online Course
NASA	National Aeronautics and Space Administration



*Climate Change Initiative+ (CCI+)  
Phase 1*

End-to-End ECV Uncertainty Budget

Ref.: ESA-CCI-PRGM-EOPS-SW-17-0032

Date: 13/09/2021

Version : v3.1

Page: 16 of 46

NOAA	National Oceanic and Atmospheric Administration
NOP	Numerical Ocean Prediction
NWP	Numerical Weather Prediction
Obs4MIPs	Observations for Model Intercomparison Projects
ODP	Open Data Portal
OOPC	Ocean Observation Panel for Climate
OTT	Ocean Target Transform
Pi-MEP	Pilot Mission Exploitation Platform
PMP	Project Management Plan
PSD	Product Specification Document
PUG	Product User Guide
PVASR	Product Validation and Algorithm Selection Report
PVIR	Product Validation and Intercomparison Report
PVP	Product Validation Plan
QA4EO	Quality Assurance Framework for Earth Observation
QSR	Quarterly Status Report
R&D	Research and Development
RTM	Radiative Transfer Model
RCP	Representative Concentration Pathways
RD	Reference Document
SAF	Satellite Applications Facility
SAR	Synthetic aperture Radar
SISS	Satellite and In situ [Working Group]
SLP	Sea Level Pressure



SMAP	Soil Moisture Active Passive [mission of NASA]
SMOS	Soil Moisture and Ocean Salinity [satellite of ESA]
SoW	Statement of Work
SRAL	SAR Radar Altimeter (of Sentinel-3)
SRD	System Requirements Document
SSD	System Specification Document
SSS	Sea Surface Salinity
SST	Sea Surface Temperature
SVR	System Verification Report
SWIM	Surface Waves Investigation and Monitoring (instrument of CFOSAT)
SWH	Significant Wave Height (see also Hs)
TB	Brightness Temperature
TBC	To Be Completed
TOPC	Terrestrial Observation Panel for Climate
TR	Technical Requirement
UCR/CECR	Uncertainty Characterisation Report (formerly known as the Comprehensive Error Characterisation Report)
UNFCCC	United Nations Framework Convention on Climate Change
URD	User Requirements Document
USB	Universal Serial Bus
USGS	United States Geological Survey
VOS	Volunteer Observing ships
WCRP	World Climate Research Programme
WGClimate	Joint CEOS/CGMS Working Group on Climate
WMO	World Meteorological Programme



***Climate Change Initiative+ (CCI+)***  
***Phase 1***

End-to-End ECV Uncertainty Budget

Ref.: ESA-CCI-PRGM-EOPS-SW-17-0032

Date: 13/09/2021

Version : v3.1

Page: 18 of 46

WS            Wind Speed  
WWA        World Wave Atlas (of FUGRO)



## 2 Sensor main characteristics

### 2.1 Introduction

---

This section presents the main characteristics of SMOS, SMAP and Aquarius sensors. It provides information about revisit time and mean footprint resolution.

### 2.2 SMOS

---

The main SMOS characteristics are:

- ✓ Interferometric radiometer with center frequency of 1.41 GHz and bandwidth of 27 MHz
- ✓ Data time coverage: 2010-now
- ✓ sub-cycle of 18 days
- ✓ Exact repetitive cycle : 149 days
- ✓ Earth Incidence Angle: 0-60°.
- ✓ Local ascending/descending time: 6 AM/PM.
- ✓ four polarizations
- ✓ 3-dB (half power) footprint size: between 40 and 100 km (according to the incidence angle)
- ✓ Global coverage : 3 days

### 2.3 SMAP

---

The main SMAP characteristics are:

- ✓ Radiometer (6-meter mesh antenna) with center frequency of 1.41 GHz and bandwidth of 24 MHz
- ✓ Exact repetitive cycle of 8 days
- ✓ aft and fore acquisition
- ✓ Data time coverage: 04/2015 to now
- ✓ Conical scanning at 14.6 rpm. Scan time: 4.1 sec
- ✓ Earth Incidence Angle: 40°.
- ✓ Local ascending/descending time: 6 PM/AM.
- ✓ four polarizations
- ✓ 1000 km wide swath.



- ✓ 3-dB (half power) footprint size: 40 km.
- ✓ Global coverage : 3 days

## 2.4 Aquarius

---

The main Aquarius characteristics are:

- ✓ Radiometer (3 beams) with center frequency of 1.413 GHz and bandwidth of 25 MHz.
- ✓ Exact repeat cycle of 8 days
- ✓ Almost global coverage : 7 days
- ✓ Data time coverage: 08/2011 to 06/2015.
- ✓ Earth incidence angles: 28.7, 37.8, and 45.6°.
- ✓ Footprints for the beams are: 74 km along track x 94 km cross track, 84x120 km and 96x156 km yielding a total cross track of 390 km.
- ✓ Measurement every 1.44s (about every 10 km).
- ✓ Distance between beam swaths of about 100 and 150 km (across track).
- ✓ Local ascending/descending time: 6 PM/AM.
- ✓ TH, TV and third Stokes
- ✓ Aligned with a scatterometer (1.26 GHz); both instruments polarimetric.



## 3 L1 uncertainty characterization

### 3.1 Introduction

---

In order to better understand the SSS uncertainties at L4, we need to have a global understanding on what happens at L0-L1 in terms of TB uncertainty budget. L0-L1 processing are very complex and require specific expertise. Indeed, it is not in our scope to review all L0-L1 processing methods for all satellite missions. Our purpose is to replay L2 from existing L1 products. It is therefore not our objective to re-estimate TB uncertainties but to take what comes out of the L0-L1 and work with them, as long as we have sufficient information to properly propagate TB uncertainties toward level 2. TBs at the L1 processing output have systematic uncertainties that are not corrected at L0-L1 and that we take into account in the higher levels in an empirical way.

Hence, we develop methods for correcting systematic uncertainties and estimating random uncertainties at SSS level coming from remaining differences between forward model predictions and TB data from SMOS, Aquarius or SMAP are still found after instrumental calibration. These differences may exhibit seasonal patterns varying from ascending to descending passes, due mainly to uncertainties in the thermal model/monitoring of the instrument, Radiative Transfer Model (RTM) inaccuracies, input auxiliary EO data , ...etc.

### 3.2 SMOS sensor

---

SMOS is an L-band interferometer that measures the Fourier transform of the scene. Level 1 processing is the passage of visibilities (which integrate antenna gains) to the Fourier transform of TB then the passage of TB in the frequency space domain to the physical space domain. These different processing require knowledge of antenna gains, with, as an additional difficulty, a spatial sampling of the observed frequencies lower than Shannon's sampling. Since the scene has infinite frequencies, this poses specific difficulties for the passage into physical space domain. In the following, this operation is called reconstruction

Complex calibrations for thermal drifts based on Noise Injection Radiometer data and several on-board thermistor measurements are used to calibrate the visibilities. Short-term calibration is regularly performed at raw level to compensate for high variability drifts. In addition, cold-sky calibration is performed at several occasions in a year when the satellite sensor is rotated upward sky during dedicated manoeuvres (used for the so-called Flat Target Transformation). Yet, systematic and seasonal image reconstruction uncertainties are still found in the reconstructed level 1 data despite raw data calibration. This can occur, for example, due to the instrument response to a very strong L-band source in the field of view, such as the sun image and its tails corrupting the quality of the reconstructed brightness but also because of image reconstruction systematic uncertainties (noise floor, aliasing, instrument impulse response function, antenna pattern uncertainties).

To compensate for these distortions in the image, a vicarious calibration is performed at level 2 by evaluating a mean spatial difference in the antenna coordinate frame between SMOS antenna



TBs and a radiative transfer forward model of the brightness obtained along specific orbits in the middle of the Pacific. The forward model is derived using climatology of SSS or analysed in situ data (ISAS fields) interpolated along the half orbits used for calibration. The Tb adjustment is named the Ocean Target Transformation (OTT).

Following this correction, it is possible to empirically validate the uncertainties on TBs against the expected radiometric noise. These uncertainties are in accordance with the expected radiometric noise, as soon as the various unmodeled contributions have been filtered (RFI, sun effect, etc.). On the other hand, there are reconstruction biases that are not corrected by the OTT, which then generates biases in the estimated parameters. For the time being, L1 processing do not make it possible to avoid such biases.

### **3.3 SMAP and Aquarius sensors**

---

To correct for residual drifts after raw data calibration, NASA algorithms thus use the median difference between Aquarius (or SMAP) data and forward radiative transfer model simulations of the brightness temperature obtained by using HYCOM model SSS or Argo SSS (depending on the release) as a forcing parameter. The difference is then averaged globally and the mean difference evaluated daily is used for post-calibration adjustments.

For SMAP (it is more complicated than for Aquarius: the SMAP antenna has some non-negligible emissivity), the antenna temperature predicted from thermal model has some uncertainties, and a latitudinal correction has to be applied.

In addition, uncertainties in the modelled side-lobes of the radiometer antenna patterns used for image reconstruction/antenna temperature provide some signal leakage of the brighter sources (land, sea ice) into the lighter source (pure ocean). These so-called “land contamination” or “ice-contamination” need to be corrected for the input TB to retrieve an unbiased SSS as close as possible from the coast lines or ice-edges. A method of contrasting half-space is currently used in NASA algorithms to adjust antenna pattern corrections when Aquarius or SMAP pass through two sharply contrasted (in the TB sense) semi-infinite surface (from sea to land, for instance).

### **3.4 RFI filtering**

---

SMOS, Aquarius and SMAP missions operate in the L-band protected spectrum (1400-1427 MHz) that is nevertheless now known to be vulnerable to radio-frequency interference (RFI). Areas affected by RFI might experience data loss or result in inaccurate soil moisture and ocean salinity retrieved values. To alleviate this situation, several strategies were put into place to filter the data from RFI perturbed measurements. As SMOS, launched in 2009, was the first satellite to operate in L-band, it does not have any on-board hardware/software to filter RFI, so that RFI filtering/mitigation only rely on data post-acquisition processing. This issue is significantly less important for SMAP (and to a least extent for Aquarius), as they are (were) equipped with on-board frequency/time-domain-based RFI filters.



***Climate Change Initiative+ (CCI+)***  
***Phase 1***

End-to-End ECV Uncertainty Budget

Ref.: ESA-CCI-PRGM-EOPS-SW-17-0032

Date: 13/09/2021

Version : v3.1

Page: 23 of 46

Over the ocean, SMOS data are contaminated by RFI emitted principally from land. The impact on the reconstructed brightness temperature can be positive or negative and is not limited to the location of the on-ground antenna causing the interference but affects measurements as soon as there is the line of sight between the instrument and the RFI source (Corbella, Martín-Neira, Oliva, Torres, & Duffo, 2012). Due to the interferometer principle from a Y-shape antenna, the contamination is not circular symmetric in SMOS images, but presents six main tails spreading from the RFI source. In the case of SMAP and Aquarius, the RFI contamination is different as they operate real-aperture radiometer and on-board data filtering with enhanced detection capabilities. To protect against RFI, Aquarius employs rapid sampling (10 ms, milliseconds) and a “glitch” detection algorithm that looks for outliers among the samples. Samples identified as RFI are removed, and the remainder is averaged to produce an RFI-free signal for the salinity retrieval algorithm. The RFI detection algorithm appears to work well over the ocean with modest rates for false alarms (5%) and missed detection but RFI are still detected in Aquarius (Le Vine and De Mattheaïs, 2014). SMAP takes a multidomain approach to RFI mitigation by utilizing an innovative onboard digital detector back end with digital signal processing algorithms to characterize the time, frequency, polarization, and statistical properties of the received signals. Almost 1000 times more measurements than what is conventionally necessary are collected to enable the ground processing algorithm to detect and remove interferences.

## 4 L2OS uncertainty characterization

### 4.1 Introduction

---

SSS random uncertainties are estimated from self-consistency analysis or by adjusting global metrics of differences between observed SSS with external data (ISAS, Argo). The random and systematic uncertainties can be obtained in a relative way by comparing averaged products from different sensors and orbit type (ascending or descending).

L2 SSS random uncertainty is first derived for open ocean data. In a second step, their estimate is updated in case of land contamination. We extract from L2 data a multiplicative factor to be applied on the SSS random uncertainties. This factor allows taking into account secondary side lobe effects or reconstruction effects affecting TB measurements close to the coast.

### 4.2 Methods

---

#### 4.2.1 Random uncertainty estimation

##### 4.2.1.1 Introduction

In this section we present three different methods which allow estimating SSS random uncertainties:

- by error propagation
- by comparing measured SSS with a reference (affected by a neglectable error)
- by self-consistency analysis

##### 4.2.1.2 Random uncertainty propagation

The basic uncertainties on salinity correspond to that provided in salinity level 2 products.

Level 2 algorithms are used to propagate the TB noise characterized by the radiometric accuracy, the uncertainty of all geophysical parameters (wind speed, surface temperature, etc.) on the salinity. The propagation methods generally assume a Gaussian statistic, a linearization of the forward model in the vicinity of the solution and least square type retrieval. The theoretical uncertainty such obtained depends on the a priori uncertainties on the parameters. In order to homogenize L2 uncertainties from the different sensors (SMOS, SMAP, Aquarius), a review of uncertainty propagation methods has been carried out. We then propose a strategy to standardize the uncertainty calculation and the a priori uncertainties to be assigned to the geophysical parameters. This strategy of standardizing the uncertainty calculation must be in phase with the standardization of the auxiliary data and the uniformization of the direct and inverse models on the set of sensors. Note that for the time being, model uncertainties (sun glint, roughness, atmospheric, galactic, dielectric models) are not propagated in L2 SSS. After that,

when computing L3 products by combining different L2 SSS, it is possible to use the L2 uncertainty in order to weight properly the SSS during the average.

Basically, the theoretical SSS a posteriori uncertainty depends on the radiometric accuracy ( $\sigma_{TB}$ ) and the uncertainty on the auxiliary data. If these two uncertainty sources are given, the SSS uncertainty also depends mainly on the sensitivity of TB according to the SSS. This sensitivity increases with the SST. This means that the SSS uncertainty,  $\sigma_{SSS}$ , increases at high latitudes. The relation is as follows:

$$\sigma_{SSS} = \sigma_{TB} \cdot \left( \frac{1}{\left| \frac{\partial TB}{\partial SSS} (SST) \right|} \right) \quad \text{Eqn 4-1}$$

This yields, according to a  $\frac{\partial TB}{\partial SSS} (SST)$  approximation for Stokes1 of  $-0.015 \cdot SST - 0.25$

$$\sigma_{SSS} = \frac{\sigma_{TB}}{0.015 \cdot SST + 0.25}$$

SSS uncertainties due to WS uncertainties and SST uncertainties could be added quadratically to this relation after propagation.

#### 4.2.1.3 Random uncertainty from external data comparison

The uncertainty balance obtained by uncertainty propagation does not generally include the uncertainties on the models themselves (model of galactic noise, roughness, solar contamination, etc.). In order to estimate the errors and to validate the uncertainties obtained by propagation, it is necessary to compare the satellite SSS data with external information (e.g. in-situ measurements). This can be done directly with SSS L2. It is however preferable to average the L2 data before comparison in order to reduce the noise level and to have an estimation of the systematic uncertainty. Hence the comparison with the external data is carried out on L2 and L3 products. This approach has been performed sensor by sensor (L2) .

#### 4.2.1.4 Random uncertainty from self-consistency analysis

The 3 sensors provide independent measurements. Three comparisons are made, depending on the period: SMOS-Aquarius over the period 2012-2015, SMOS-SMAP over the period 2015-2020 and SMOS-SMAP-Aquarius over the period April to June 2015. Note that if we standardize the direct and auxiliary data, the random and systematic uncertainties on the SSS data will not be completely independent. On the other hand, this could make possible to qualify uncertainties related to the unexpected behaviour of the instruments (drift, problem of reconstruction, contamination by RFI, etc).

Finally, it is possible to compare SSS by triple collocation by adding the in-situ data products. The difficulty of this inter-comparison lies in the fact that the spatial resolution of SSS in situ and satellite are not identical (representativity uncertainty to be taken into account) and that the satellite salinities are affected by correlated uncertainties (due to the use of common auxiliary data). However, it is possible to estimate a minimum uncertainty level on the sensors.

#### **4.2.1.5 Qualitative estimation of random uncertainty and identification of outliers**

In some cases, we know that the estimation of the random uncertainties at L2 is inaccurate (especially if one identifies problems of convergence in retrieval algorithms). In this case, it is important to identify the outlier SSS and flag it accordingly. In addition, some statistical indicators for TB residues may show that the uncertainty obtained by propagation is underestimated. It is then possible to empirically re-evaluate the SSS random uncertainties upwards.

### **4.2.2 Systematic uncertainty estimation**

#### **4.2.2.1 Introduction**

Estimating systematic uncertainties is much more difficult than estimating random uncertainties. In fact, in most Level 2 products, the systematic uncertainty is not directly estimated. There are two types of systematic uncertainties: relative systematic differences (inter-sensor or intra-sensor) and absolute systematic uncertainties (in comparison with 'truth'). The systematic uncertainties should be corrected with identical techniques for the 3 sensors, this being an essential prelude before combining the data of the various sensors.

#### **4.2.2.2 Estimation of relative systematic differences**

The solution to this problem is not to estimate absolute SSS, but rather to analyse salinity anomalies. This approach has been applied to SMOS and has yielded very good results (Boutin et al, 2016). In particular, specific algorithms allow correcting the relative across track systematic uncertainties (Kolodziejczyk et al. 2016) and ascending-descending latitudinal biases (Boutin et al. 2018). This type of algorithm will be extended to the other sensors and it will thus be possible to estimate the relative biases for all the sensors.

Moreover, the bias also depends on the operating point and the sensitivity of TB to SSS. Some biases related to TB bias can be corrected a posteriori, for example in relation to SST.

In order to characterize the bias, we can distinguish 2 types of bias:

- a land-sea contamination bias independent of time which is related to the instrument function (reconstruction problem for SMOS and pollution by the existence of side lobes for SMAP and Aquarius). Even though the land emissivity is expected to vary seasonally, it is so large compared to ocean emissivity ( $\sim$ a factor 2) that at first order it can be considered as constant.

- a seasonal latitudinal bias that depends on sun and galactic noise contamination and possibly on other instrumental drifts that are considered here periodic over a period of one year. In CCI+SSS v3, this correction is applied only on SMOS data, but it could be applied on other sensors in future versions.

We consider that latitudinal bias is independent of the basin (Atlantic, Pacific or Indian Ocean) and that it applies in addition to coastal bias in an additive way.

The general formulation of the bias, for a given grid node at the position (lat,lon) is as follows:

$$SSS_{obs}(X, t, orb, lat, lon) = SSS(t) - bc(X, orb, lat, lon) - bl(X, orb, t\_month, lat) \quad \text{Eqn 4-2}$$

with bc, coastal bias and bl latitudinal bias. SSS\_obs is the observed salinity, SSS(t) corresponds to the unbiased SSS. X corresponds to a subset of data that is assigned in the same way through the bias. In the case of Aquarius, this may be the considered antenna beam or, in the case of SMOS, the position of the measurement in the swath, in the case of SMAP the aft and fore views. As already mentioned, bl is not considered for Aquarius and SMAP in CCI+SSS v3.

It is possible to calculate bc and bl independently starting with the calculation of bl on open sea areas taken far from the coast. Then, a latitudinal correction is applied to the coastal pixels. From these latitudinal bias corrected data, we can estimate bc. Since the number of independent subsets of data is relatively large, the different biases can be estimated in a self-referenced way, i.e. there is no need for an external reference when considering anomalies and not absolute salinities. Note that the Eqn 4-2 requires a simultaneous estimation of SSS(t) (or anomalies with respect to a reference salinity given by the measurements themselves) and biases bc and bl since we do not use an external reference that gives us SSS(t). This is a very important point because, in this situation, we estimate the L4 products, represented by SSS(t) at the same time as we characterize the biases. The uncertainty propagation occurs at the time of this estimate. In view of this remark, an estimation method should be proposed. We have chosen to perform a Bayesian least square method that includes a time correlation length. We can process each grid node independently of each other and thus maintain the native spatial resolution of the sensors.

The resolution of this equation will follow the method described in the paper by Kolodziejczyk et al. 2016 which presents an application on SMOS.

An improvement of this correction has been proposed, in particular as regards the inclusion of SST. This approach remains valid for all L-band sensors.

The correction of the inter-dwell or latitudinal instrument bias does not depend in principle on geophysical conditions. However, if the brightness temperature bias ( $\Delta TB$ ) is generally independent of geophysical conditions and especially of the sea surface temperature (SST), this is not the case for the SSS bias ( $\Delta SSS$ ) ([RD09]). Indeed, the sensitivity of the retrieval (transition from brightness temperatures to SSS) depends strongly on SST. The sensitivity of TB to SSS decreases with a decrease in SST. Therefore, a given  $\Delta TB$  bias will not have the same impact on SSS at low or high temperatures. More precisely, we have:

$$\Delta SSS = \Delta TB \cdot \left( \frac{1}{\frac{\partial TB}{\partial SSS}(SST)} \right)$$

The lower the sensitivity  $\frac{\partial TB}{\partial SSS}(SST)$ , the greater the bias on the SSS, for a constant TB bias. This behaviour obviously does not simplify the management of bias correction in SSS since, at a given point, SST can vary greatly from one season to another.

If we measure an SSS bias at SST=SST0, it is like measuring a different SSS bias at SST=SST1:

$$\begin{aligned} \Delta SSS(SST = SST1) &= \Delta SSS(SST = SST0) \left( \frac{0.015 SST0 + 0.25}{0.015 SST1 + 0.25} \right) \\ &\equiv \Delta SSS(SST = SST0) \cdot \text{coeff}_{SST0}(SST1) \end{aligned}$$

$\text{coeff}_{SST0}(SST1)$  represents the multiplicative coefficient to be applied to the calculation of the bias when it is observed at a different SST. So the idea is to compute the bias for a given SST, that is, to reduce, for each measure, to an average SST that does not necessarily correspond to the SST observed at the time of the acquisition.

#### 4.2.2.3 Estimation of absolute systematic differences.

The estimation of SSS(t) from Eqn 4-2 is affected by a global bias and the SSS(t) estimate contains essentially the SSS anomalies. The relative correction described in the previous section does not allow reaching absolute SSS field.

The absolute systematic uncertainty calculation requires correction based on climatology or in-situ data. At SSS level, the resolution of Eqn 4-2 gives L4 SSS anomalies. At this level, it is possible to add at these SSS anomalies a constant shift in order to reach an absolute SSS.

### 4.3 Spatial sampling

The definition of the grids on which the SSS are projected can be done at several levels:

1/ from user considerations who wish to work on regular rectangular grids in (lat,lon), oversampled.

2/ from pragmatic considerations related to information content. In this case, it is a question of working on a grid that allows to switch to any other grid with a minimum loss of information. Given the resolution of the sensors, it is a question of sampling at a frequency twice as high as the resolution. The average resolutions of SMOS, SMAP and Aquarius are respectively ~50 km, 40 km and 150 km. A 0.25° longitudinal sampling should then allow interpolation on any grid. The EASE grid is an area conservative grid (Figure 1), regular in degrees of longitude but not in latitude with an average sample length of 25 km [Brodzik *et al.*, 2012]. The level 2 SSS is resampled on this grid before analysis

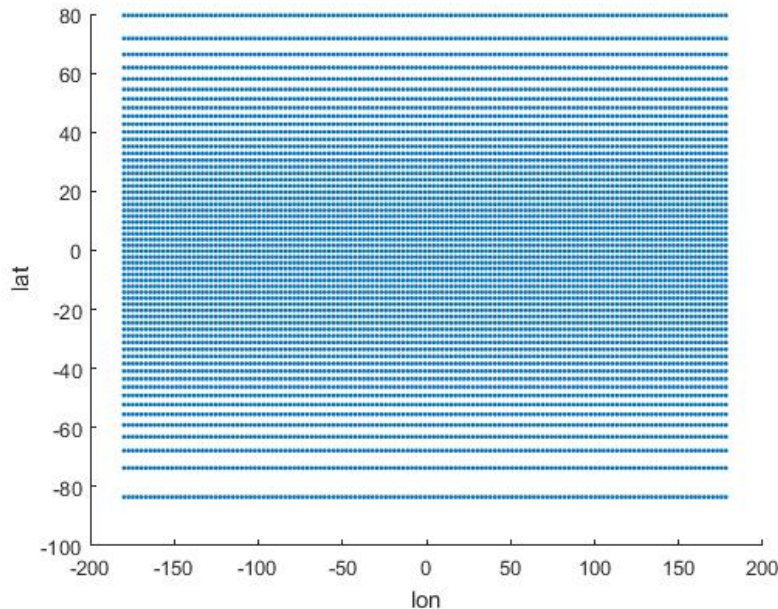


Figure 1: EASE grid (under sampling of a factor of 10).

## 4.4 Uncertainty estimation methods applied to SMOS, SMAP and Aquarius.

### 4.4.1 Introduction

We use L2 and L3 products to characterize the uncertainty on the SSS estimator and get a first idea of the bias behaviour for each sensor.

### 4.4.2 PI-MEP (from <https://www.smos-pimep.org/overview.html>)

The Soil Moisture and Ocean Salinity (SMOS) mission was launched on 2nd November 2009 as the second Earth Explorer Opportunity mission within ESA's Living Planet programme. It has been continuously providing brightness temperature data in L-Band since January 2010, which are used to retrieve Soil Moisture (SM) and Sea Surface Salinity (SSS) data over land and ocean, respectively. This project funded by ESA aims at setting up a Pilot Mission Exploitation Platform (Pi-MEP), focussing on ESA's SMOS mission and supporting enhanced validation and scientific process studies over ocean.

Pi-MEP project objectives:

- Focus 1 - Enhanced validation of satellite SSS and products assessment
- Focus 2 - Oceanographic exploitation and case-studies monitoring



The **Pi-MEP** is designed to allow **systematic comparisons between available datasets** by providing **comparable QC metrics** for all these SMOS data derived SSS products, as well as for the two other NASA missions. This will enable:

1. the user to choose which satellite SSS product is best adapted for their own specific application,
2. to improve the Level 2 to Level 4 SSS retrieval algorithms by better systematically identifying the conditions for which a given SMOS, or other satellite, SSS products are of good or degraded quality.
3. to in fine converge towards best approaches and generate less but better satellite SSS products.

A large ensemble of **in situ SSS data distributed by different data centers** can be used to infer SMOS, Aquarius or SMAP SSS data product quality. This includes in situ data from the following sources:

- **ARGO float data** (CORIOLIS)
- **Moored buoy data** (TAO, PIRATTA, RAMA, STRATUS, NTAS, SPURS1-2, WHOTS)
- **Thermo-Salinograph** data installed on Voluntary Observing Ships (LEGOS, SAMOS)
- **Thermo-Salinograph** data installed on Research Vessels (GOSUD, Polarstern, NCEI-0170743)
- **Thermo-Salinograph** data installed on Sailing Ships (GOSUD)
- **Surface Drifters** (LOCEAN)
- **Equipped marine mammals** (MEOP)
- **Analysed in situ data fields** (IFREMER/LOPS)
- **Dedicated Campaign data** (e.g. SPURS)

So the PI-MEP is very useful in order to estimate the quality of the L2OS and L3OS products.

#### 4.4.3 External data

In order to compare the SSS of the different sensors with external data, we will use the ISAS data and the different comparisons made at PI-MEP. It should be noted that ISAS data are very spatially smoothed (600 km) which can lead to interpretation difficulties when comparing better spatially defined satellite fields over areas where spatial variability is high. In this case, the representativity uncertainties are significant in the comparison mechanism. This representativity uncertainty could be calculated on the basis of high spatial resolution models.

#### 4.4.4 Data analysis

##### 4.4.4.1 Introduction

Data analysis is essentially carried out on the basis of self-consistency of SSS.



A first understanding of the L2 SSS uncertainties comes from the ATBDs and validation reports of each sensor.

Random uncertainties must be well known in order to be able to properly weight the different SSSs when developing L3 and L4 products. We propose to validate the theoretical uncertainties provided in the products or to empirically estimate the uncertainties that affect the SSS estimator (in the case of SMAP L2C products and Aquarius L3 products, such uncertainties are not provided). We know that the theoretical uncertainty (which assumes that the direct model and instrumental response are known) depends essentially on radiometric measurement errors and the sensitivity of TBs to SSS. This sensitivity depends essentially on the sea surface temperature SST. We will therefore attempt to characterize the theoretical uncertainty according to SST.

With regard to systematic uncertainties, there are several causes that generate them:

-the instrument, which is known with a certain level of precision, undergoes poorly controlled and therefore poorly corrected solicitations (antenna temperature, antenna gains, etc.).

-the direct model used for inversion is not perfect (dielectric constant, sun, galactic, TEC...)

In all cases, systematic uncertainties result from limited knowledge of the signal and sensor.

Currently, the various sensors have their own correction strategies for brightness temperatures.

However, as we will show, there are residual biases in salinity. Here, we are trying to build a salinity field from salinities from the different sensors. The aim is to mix SSS as homogeneous as possible and thus to correct inter-sensor bias.

Two possibilities for addressing these residual biases:

-to improve knowledge of the signal and sensors and to act on brightness temperatures and direct models.

-to compute empirically the bias and to correct it afterwards.

These biases affect the data differently depending on the across-swath position and the orbit type (ascending or descending). More precisely, we know that glint effects depend on the season and the geometry of observation. There are a solar glint and a galactic glint which can, depending on geometry and latitude, have a greater or lesser impact on the signal. Similarly, the flux affecting the antenna back lobes depends on the orientation of the antennas and the position of the different sources and their intensity (for instance, even if the back lobe gains are very low, a source like the sun can affect significantly the total signal).

We consider that a constant bias affects the following subsets of measurements:

- for SMOS, the same bias is considered for all SSS coming from the same dwell line and the same position (lat,lon). The dwell lines are sampled across track every 25 km. The bias has two components : a time-independent component and a latitudinal seasonal component.

- for SMAP, the bias is considered independently for fore and aft measurements and for each (lat,lon) position.

SSS from ascending and descending orbits are also differentiated for both sensors.

- for Aquarius, we will use the L3 data, ascending and descending orbits separately.

Therefore, we have several datasets from the different sensors and it is necessary to solve the Eqn 4-2 in order to estimate the biases  $b_c$  and  $b_l$  for SMOS As underlined in section 4.2.2.2, the estimation of the biases is done simultaneously with the SSS optimal interpolation.

#### 4.4.4.2 SMOS L2OS data

The SMOS data comes from a specific L2OS CCI processing. This processing used L1 v6 data (gibbs 1 processing) as input. The OTT are computed by using ISAS and the a priori information on the auxiliary parameters comes from ERA5. The forward models are those implemented in the L2OS v662 processor, except for the dielectric constant model which is new and has been derived from SMOS data by Boutin et al. (2020). The data are corrected from instantaneous rain rate lower than 10mm/h by using A. Supply relationship (2020). For higher rain rate value, the data are discarded.

##### 4.4.4.2.1 Estimation of random uncertainty by propagation in the L2OS processor

A maximum-likelihood Bayesian approach is used in the L2 inversion algorithm, taking advantage of the a priori information available about geophysical parameters (SSS, SST, wind speed, TEC, etc.), hereafter denoted  $P_i$ . With this formalism, errors on TB and on the retrieved geophysical parameters are assumed to be Gaussian. The following cost function  $\chi^2$  is minimized:

$$\chi^2 = \sum_{i=1}^N \frac{[A_{meas\ i} - A_{model\ i}]^2}{\sigma_{Ai}^2} + \sum_{j=1}^M \frac{[P_{j0} - P_j]^2}{\sigma_{Pj0}^2}$$

This means that the uncertainty on the a priori  $P_{j0}$  (WS, SST ...) parameters are propagated on the SSS estimator.

The theoretical a posteriori variance (uncertainty)  $\sigma_{P_i}^2$  can be computed by the Levenberg-Marquardt algorithm as follows (Zine et al., 2008):

$$\begin{bmatrix} \sigma_{P1} \\ \dots \\ \sigma_{PM} \end{bmatrix} = \sqrt{diag(\mathbf{M}^{-1})}$$

where  $\mathbf{M}$  is the pseudo-Hessian, with  $\mathbf{M} = \mathbf{F}^T \mathbf{C}_0^{-1} \mathbf{F}$ , where  $\mathbf{C}_0$  is the *a priori* covariance matrix and  $\mathbf{F}$  the matrix of derivatives:

$$diag(\mathbf{C}_0) = \begin{bmatrix} \sigma_{A1}^2 \\ \dots \\ \sigma_{AN}^2 \\ \sigma_{P10}^2 \\ \dots \\ \sigma_{PM0}^2 \end{bmatrix}$$

The two components of this *a priori* covariance matrix  $\mathbf{C}_0$  are:

- $\sigma_{An}^2 = \sigma_{Ameas,n}^2 + \sigma_{Amodel,n}^2$  which includes  $\sigma_{Ameas,n}^2$ , the estimated instrument brightness temperature uncertainty, and  $\sigma_{Amodel,n}^2$  the estimated forward model uncertainty. Both are considered in the antenna reference frame. The radiometric uncertainty  $\sigma_{Ameas,n}^2$  is already given in the antenna reference frame. The model uncertainty  $\sigma_{Amodel,n}^2$  is given in the ground reference frame and propagated to antenna frame before the retrieval (using the ground to antenna rotation matrix, see Appendix B of Zine et al., 2008).
- $\sigma_{PMi}^2$ , the *a priori* variance of the geophysical parameter  $P_{Mi}$

Providing the L2OS users with an improved uncertainty  $\sigma$  is key for a number of application, such as proper L2 SSS merging at Level3 and 4 ( $\sigma$  can be used to properly weight multiple L2 SSS observations in a specific space-time window), or for assimilation into Ocean General Circulation models, etc.

Typically,  $\sigma_{Ameas,n}^2$  ranges from 1.5 to 3.5 K depending on the distance to the sub satellite point. Radiometric accuracy is computed based in two main parameters: integration time of the snapshot and footprint size, or the equivalent area introduced into the computation of the measurement in the Fourier space. This means that it depends on incident angle and, therefore, there is a cross-track dependency/variation, but also there is dwell line dependency. In a first approach, we took the model uncertainty  $\sigma_{Amodel,n}^2$  to be constant and equal to 0.5 K for H and V polarization and 0.1 K for Stokes-3 and Stokes-4. In addition, in the current version of the processor (v662), the geophysical parameter *a priori* uncertainties are constant as function of time and space and given as follows:  $\sigma_{SSS} = 100$  psu;  $\sigma_{SST} = 1^\circ\text{C}$ ;  $\sigma_{WS} = 2$  m/s and  $\sigma_{TEC} = 10$  TECu.

A first improvement has been done by multiplying SSS *a posteriori* uncertainty by  $\chi$ , which is the normalised square root of the cost function  $\chi^2$  after convergence.

#### 4.4.4.2 Estimation of random uncertainty by using empirical approach

In order to estimate the actual uncertainties empirically, we consider, for each grid node, time series of 40 days of data taken at different times of the year. The SMOS revisit time being about

4 days, we have about ten SSS over this period. Assuming that the SSS does not change over this period (which is true most of the time), the std of the time series gives an idea of the uncertainty. However, the uncertainty depends on the position of the measurement according to the center of the swath. In order to normalize the data, we create a reduced dimensionless centered variable X (normalizing by the theoretical uncertainty a posteriori  $\sigma_{SSS}$  multiplied by the  $\chi$ ):

$$X = ((SSS - \langle SSS \rangle) / \widetilde{\sigma}_{SSS}) \quad \text{with} \quad \widetilde{\sigma}_{SSS} = \sigma_{SSS} \times \chi$$

This new random variable should follow a Gaussian distribution of mean 0 and standard deviation 1 if the theoretical uncertainty is realistic. If the theoretical uncertainty is underestimated, the std of this new variable is greater than 1. In this way it is possible to homogenize SSS affected by different theoretical uncertainties.

The histograms of the reduced centred variable are presented in Figure 2, and we note that the distributions are very close to a Gaussian of zero mean and standard deviation 1. The relatively high values of the standard deviation (1.8 and 1.25) are mainly related to distribution tails and the sensitivity of the std to outliers. We can see that for the open sea, the theoretical uncertainty weighted by the  $\chi$  gives results very close to the error. For the coast, there are still high uncorrected contaminations. They are dominant in the vicinity of the Asian coast where RFIs are very strong and not temporally stable. In some regions, the high value of the std is due to the dynamics of the SSS over 40 days (rainy areas such as ITCZ, river plumes). In this case, the stability assumption of the SSS is not ensured.

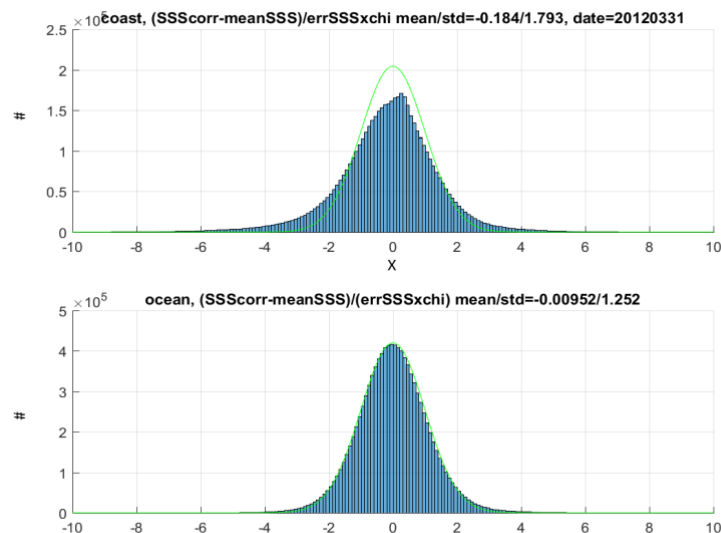


Figure 2: histogram of the new random variable X (reduced centered SSS) after applying a coastal correction. Top: pixels near the coast (dcoast < 400 km); bottom: pixels in the open ocean. March 2012.

So, to conclude, the SMOS theoretical uncertainty multiplied by the adjustment  $\chi$  in some cases, is underestimated, especially on the Asian coast and places heavily contaminated by RFIs. This

indicates the presence of outliers. The algorithm of Boutin et al. 2018 allows us to get rid of some of these outliers by adding a 3 sigma filter from data intercomparison.

Close to the coast, a specific CCI processing is implemented by multiplying the theoretical uncertainty by a factor depending on the distance to the coast  $f(\text{dist})$  (see Figure 3).

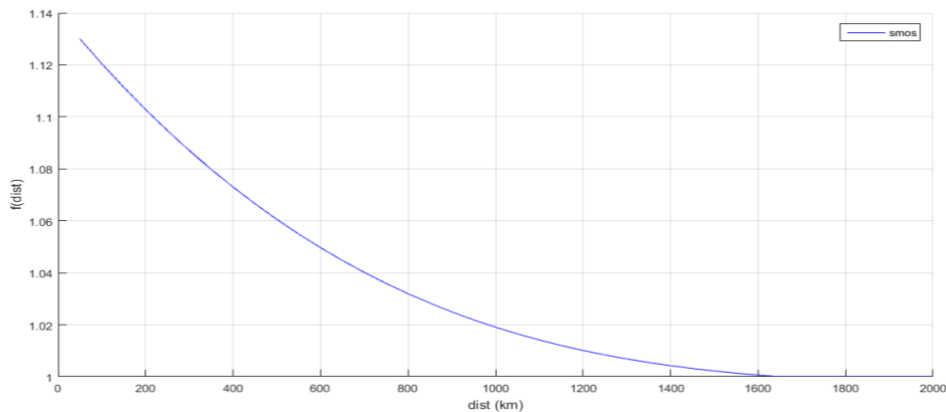


Figure 3: uncertainty factor according to the distance to the coast.

#### 4.4.4.2.3 Estimation of systematic uncertainty

N. Kolodziejczyk et al. 2016 showed that SSS biases affecting SMOS data are dependent on position on FOV and (lat,lon) so we computed an SSS bias dependence on dwell-line and position (lat,lon), see Figure 6 and Figure 7.

Also, a bias depending on latitude and season was quantified (Boutin et al. 2018). We are therefore in the situation of Eqn 4-2 with 2 biases to manage (latitudinal and inter dwell biases).

SMOS data is affected by latitudinal and coastal systematic uncertainties (biases).

The latitudinal bias was estimated under the following conditions:

- Period [2013-2019].
- Pseudo-dielectric constant (Acard) filtering ( $|\text{Acard}_{\text{smos}} - \text{Acard}_{\text{mod}}| < 3$ ). This filtering allows removing part of the ice and RFI contaminations.
- Filtering of SSS with large random uncertainty (L2 SSS random uncertainty  $< 5$ )
- Filtering of SSS which pertains to outside reasonable interval ( $\text{SSS} > 42$  or  $\text{SSS} < 5$ )
- Distance to the coast  $> 600\text{km}$ . Exclusion of some oceans. The selected area for latitudinal computation is given Figure 4.
- Smoothing of the correction with a  $5^\circ$  latitude window width (instead of  $10^\circ$  in version 1)

- Reference SSS from ISAS: isas15allinsitu + ISAS 6.2 NRT (instead of ISAS 6.2 NRT in version 1)
- Selection of ISAS SSS explaining a significant amount of variance (with PCTVAR < 80%)

An example of bias estimation is given Figure 5.

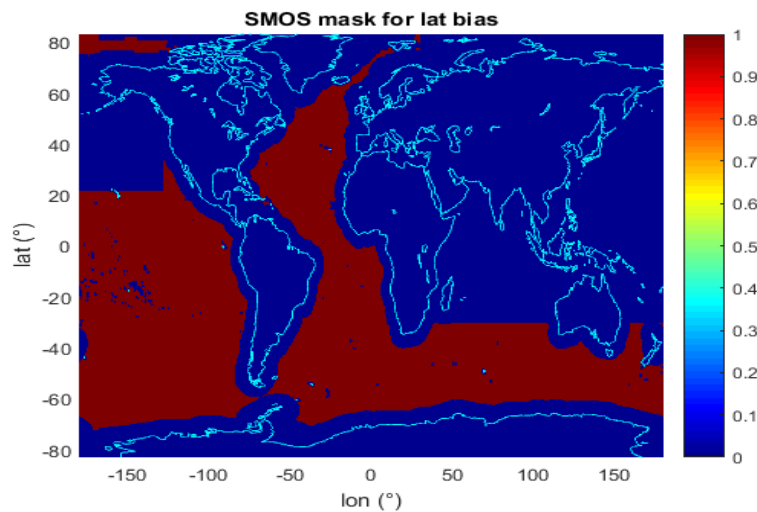


Figure 4: Mask applied to SMOS data for latitudinal bias computation.

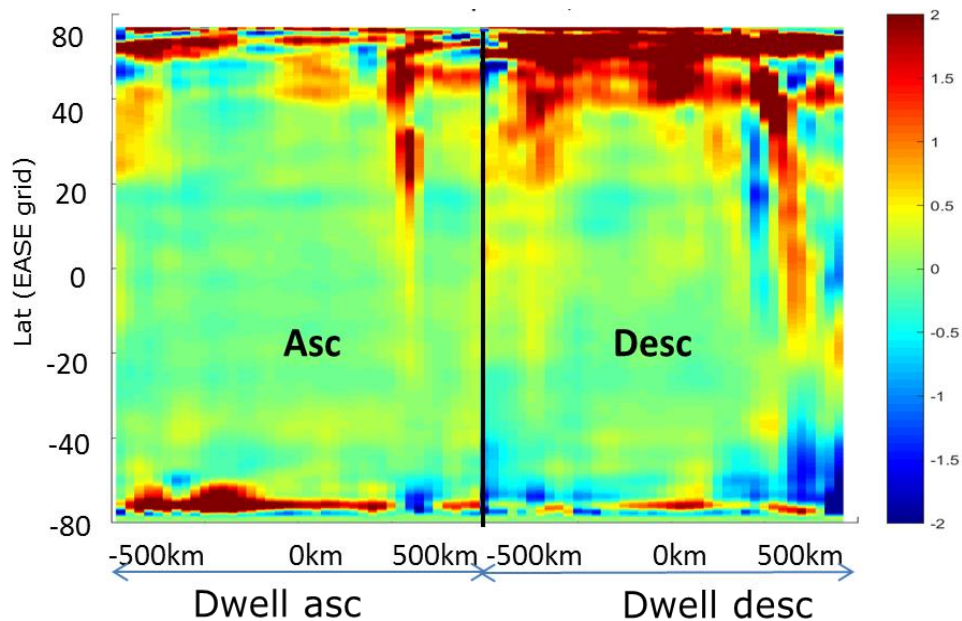


Figure 5: example of latitudinal correction for the month of January. The x axis corresponds to the ascending dwell lines and the descending dwell lines, the y axis corresponds to the latitude. Such a diagram is available for each month of the year (12-month periodicity).

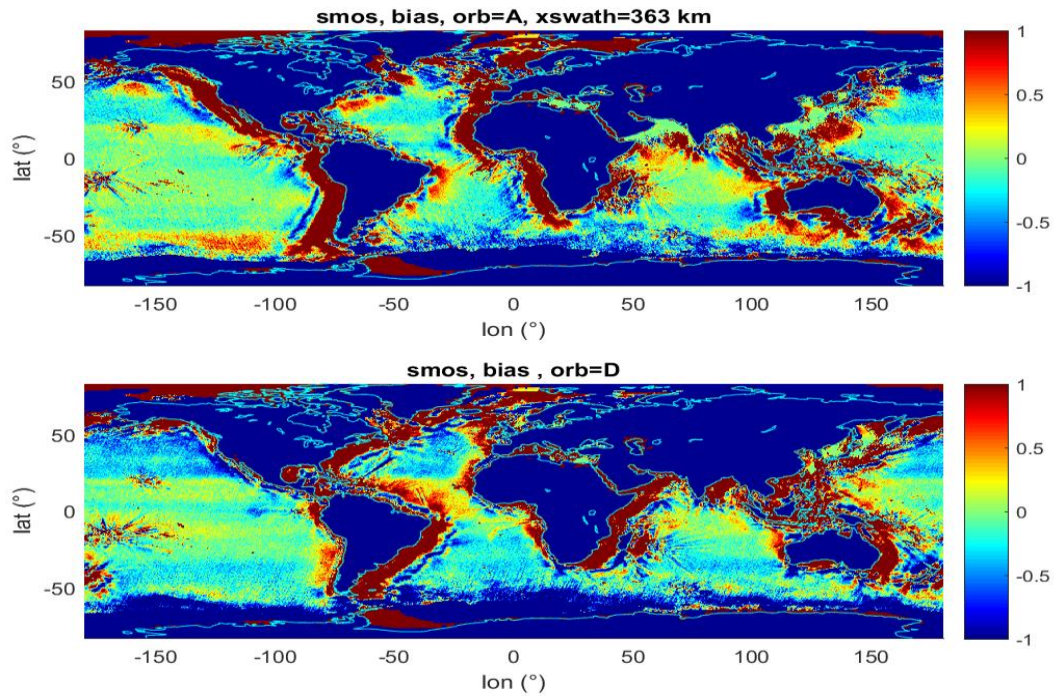


Figure 6: example of SMOS bias (relative +absolute) calculated for xswath=363 km. Top: ascending orbits; bottom, descending orbits.

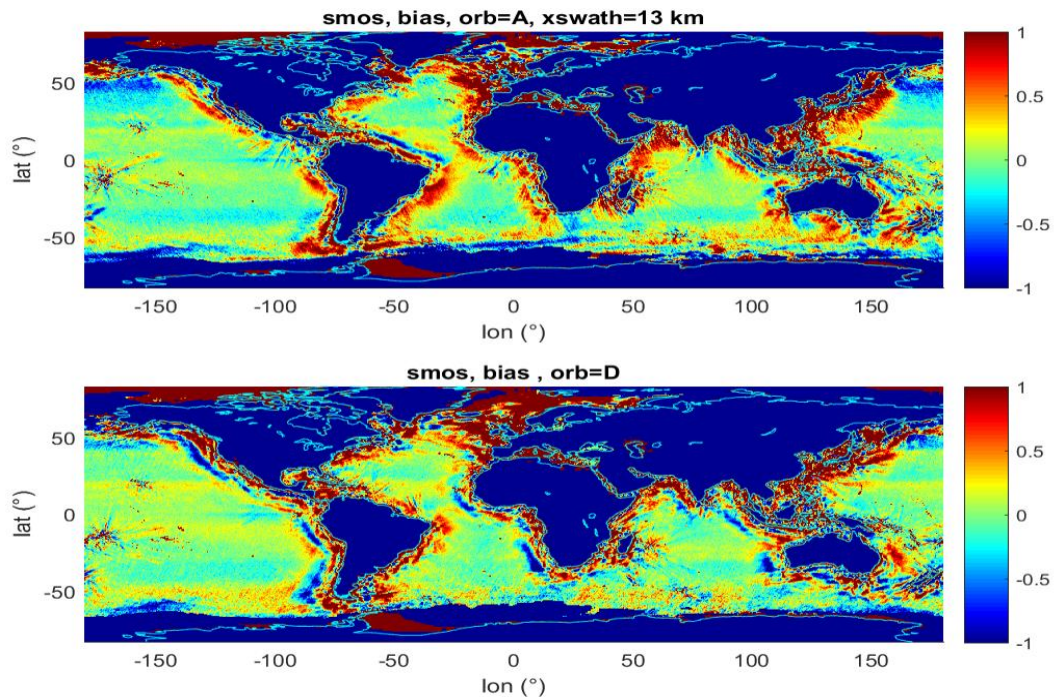


Figure 7: example of SMOS bias (relative +absolute) calculated for xswath=13km. Top: ascending orbits; bottom, descending orbits.

#### **4.4.4.2.4 flagging the data**

We chose to apply the SSS filtering before merging and correcting for relative and absolute biases, so that to remove most of the pixels with SSS outside reasonable oceanographic range, contaminated by ice or by RFI, or contaminated by high wind speed:

- SSS associated to wind speed larger than 16 m/s has been removed.
- SSS associated to pseudo-dielectric constant (Acard) is kept only if  $|Acard_{smos} - Acard_{mod}| < 2$  and  $Acard > 42$ . This filtering allows removing part of the ice and of the RFI contamination.
- SSS is kept if  $SSS > 2$  &  $SSS < 45$
- SSS is removed if  $\chi > 3$  or SSS random uncertainty  $> 3$ .
- SSS is removed if the acquisition occurs too far from the track :  $abs(xswath) > 400km$ .
- SSS is kept if  $fg\_outlier = 0$  ( $fg\_outlier$  is raised at L2OS if the number of TB outlier data are lower than a given threshold).

#### **4.4.4.3 SMAP L2 data**

We used SMAP L2C v4.0 products (SMAP\_RemSSS\_Release\_V4.0), SSS at 40 km resolution.

##### **4.4.4.3.1 Estimation of random uncertainty**

An empirical estimation is performed for SSS L2 uncertainty estimate (see [AD 06]) by using self-consistency approach. For SMAP, it is possible to compare SSS coming from aft and for acquisition and to compute the std of the difference which should be an estimator of the SSS random uncertainty multiplied by  $\sqrt{2}$  (assuming that the random uncertainty according to SST is the same for aft and for acquisition). This yields the relationship of the SSS uncertainty according to the SST shown Figure 8. This empirical uncertainty is used during the SMOS-SMAP-Aquarius merging in order to weight the SMAP SSS. This uncertainty is derived far from coast in order to avoid land and RFI contamination effect.

As for SMOS, a specific processing is implemented by multiplying the previous empirical uncertainty (obtained far from coast) by a factor depending on the distance to the coast  $f(dist)$  (Figure 9). This factor has been obtained by comparing the open ocean uncertainty with an estimation of the error according to the coast distance. Indeed, coast contaminations are expected due to secondary lobe and RFI.

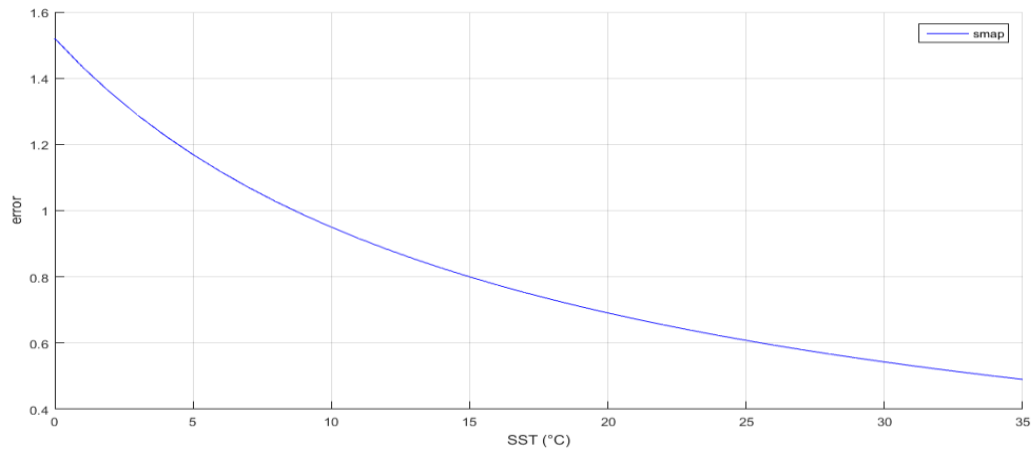


Figure 8: SSS SMAP uncertainty obtained by comparing aft and fore acquisitions.

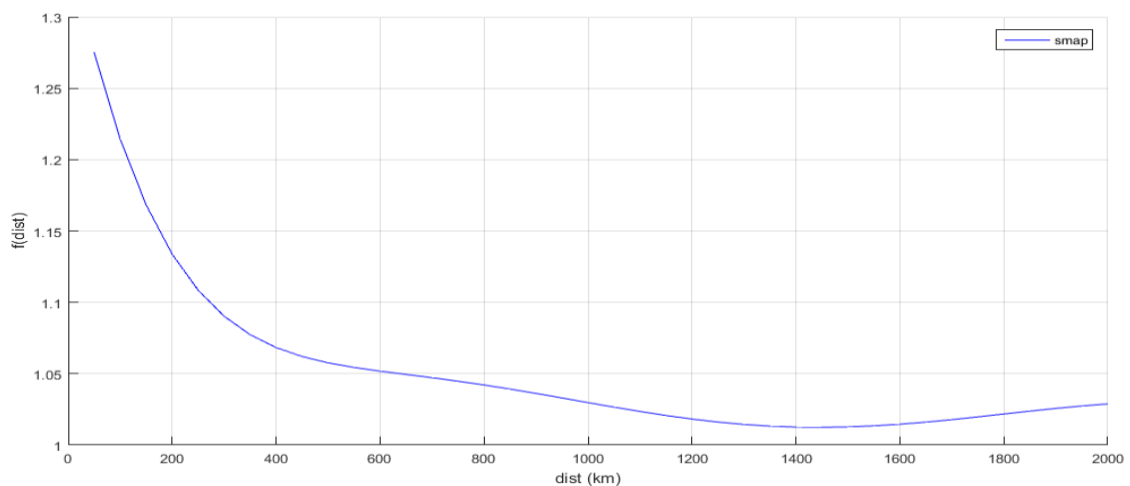


Figure 9: uncertainty factor according to the distance to the coast. SMAP.

#### 4.4.4.3.2 Estimation of systematic uncertainty

CCI latitudinal correction is not performed on SMAP SSS because such a correction is already done in the v4.0 products.

Inter calibration corrections are computed by distinguishing aft and fore acquisitions for ascending and descending orbits separately. The corrections to be applied are shown Figure 10 and Figure 11.

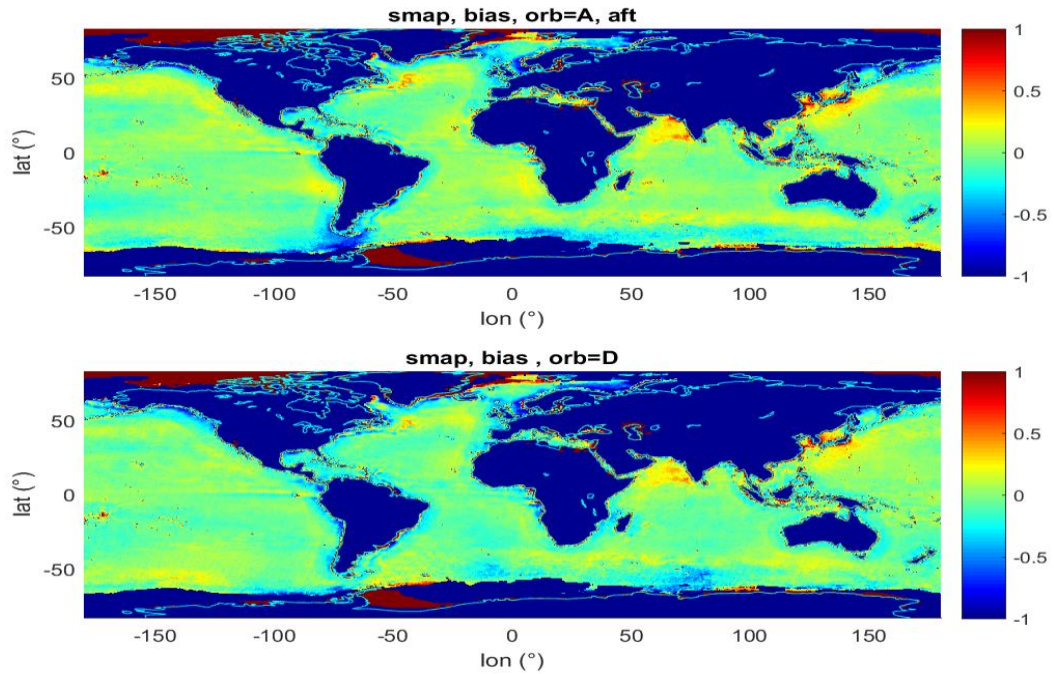


Figure 10: SMAP bias (relative +absolute) calculated for aft acquisitions. Top: ascending orbits; bottom, descending orbits.

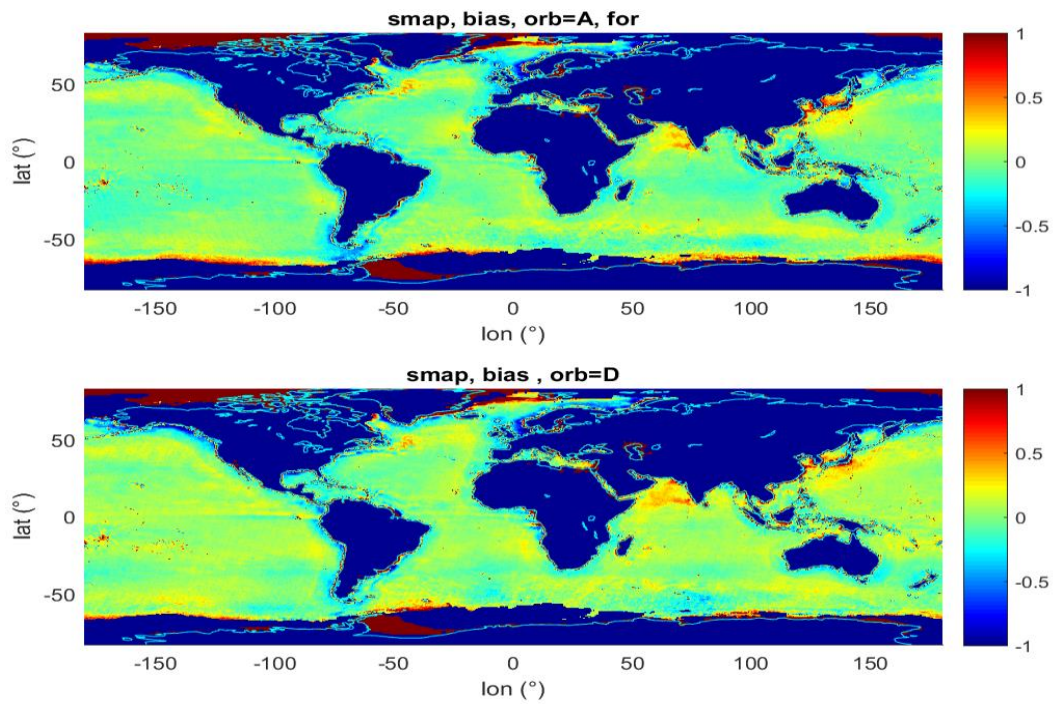


Figure 11: SMAP bias (relative +absolute) calculated for fore acquisitions. Top: ascending orbits; bottom, descending orbits.



#### **4.4.4.3 flagging the data**

We used an analogous filtering as the one used by RSS team (RD10):

- The sun glint angle is less than 50° and the azimuthal look angle lies between 30° and 50° (bit 5 in L2 Q/C flag is set).
- The moon glint angle is less than 15° (bit 6 in L2 Q/C flag is set).
- The v/h-pol average of the reflected galactic radiation exceeds 2.0 K (bit 7 in L2 Q/C flag is set).
- The TB consistency, which is defined as the  $\sqrt{\chi^2}$  of the MLE in the salinity retrieval algorithm, exceeds 1.0 K (bit 10 in L2 Q/C flag is set).
- The gain weighted land fraction exceeds 0.01.
- The gain weighted sea ice fraction exceeds 0.001.
- WS<16m/s
- SSS removal if associated to an instantaneous rain rate larger than 0.5 mm/h (no correction applied as for SMOS).

#### **4.4.4.4 Aquarius L3 data**

The following dataset is used: RSS L3 v5, ascending and descending separated products.

##### **4.4.4.4.1 Estimation of random uncertainty**

The random uncertainties can be calculated by comparing the SSS at time t with the SSS at time t+7days due to the 7-day periodicity of the satellite orbit. It is assumed that SSS on the open ocean does not change significantly in 7 days. The standard deviation of the difference then gives a fairly precise idea of the random uncertainties (multiplied by sqrt (2)). Figure 12 shows the standard deviation as a function of SST obtained far from coast.

As for SMOS and SMAP, a specific processing is implemented by multiplying the previous empirical uncertainty (obtained far from coast) by a factor depending on the distance to the coast f(dist) (Figure 13). This factor has been obtained by comparing the open ocean uncertainty with an estimation of the error according to the coast distance. Indeed, coast contaminations are expected due to secondary lobe and RFI.

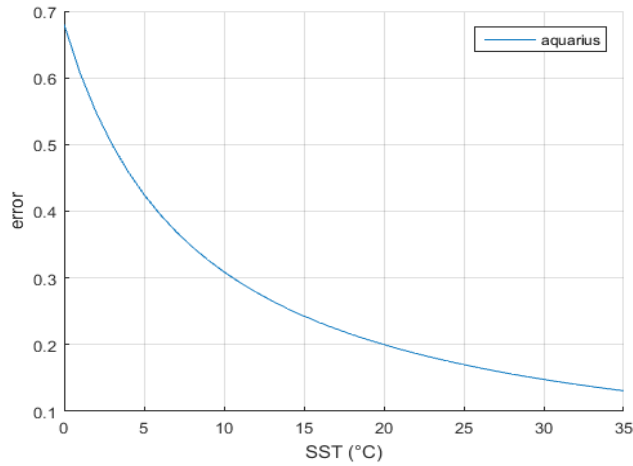


Figure 12: SSS Aquarius uncertainty obtained by comparing 7 day acquisitions.

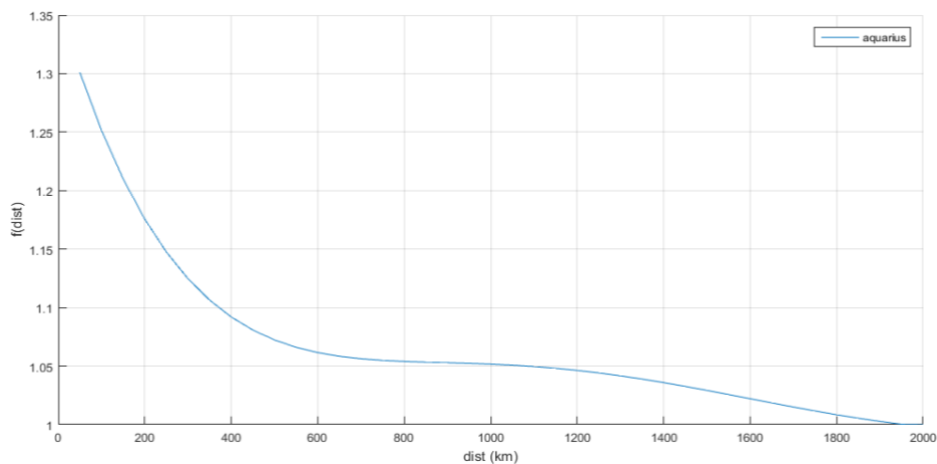


Figure 13: uncertainty factor according to the distance to the coast. Aquarius.

#### 4.4.4.2 Estimation of systematic uncertainty

Given that there is already a correction implemented in the Aquarius processing, no extra correction is added with regard to the latitudinal component of the bias. Nevertheless, the difference (SSS Aquarius - SSS ISAS) is used to verify the latitudinal bias. We observe residual biases at high and intermediate latitudes but with relatively small amplitudes compared to those observed with SMOS (Figure 14).

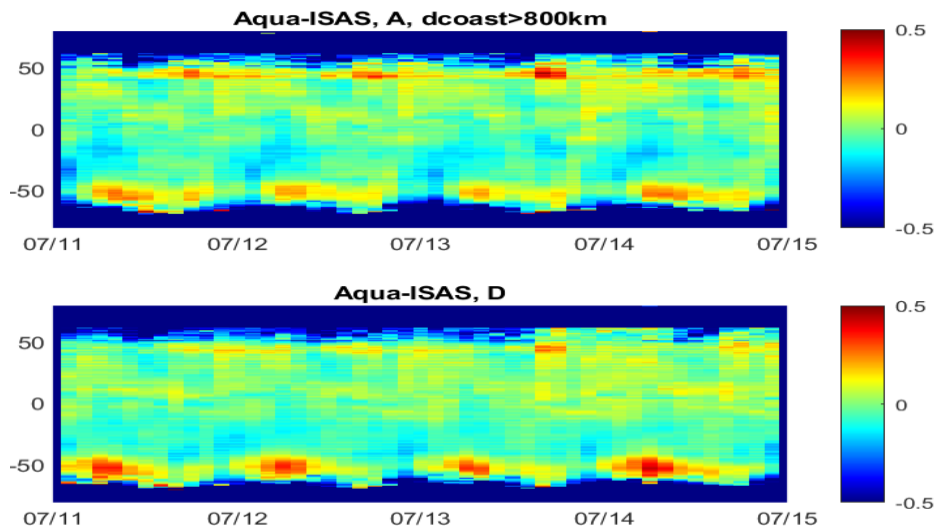


Figure 14: Hovmöller diagram of Aquarius latitudinal biases (SSS Aquarius - SSS SMAP). Top: ascending orbits. Bottom: descending orbits.

Inter calibration corrections are computed by distinguishing ascending and descending orbits separately. The corrections to be applied are shown Figure 15.

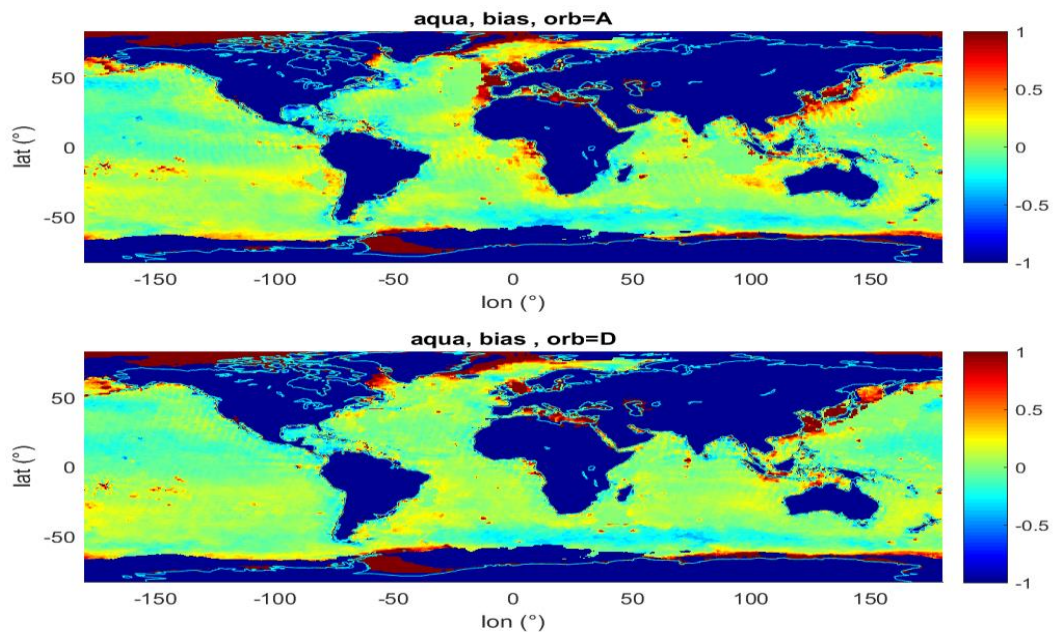


Figure 15: Aquarius bias (relative +absolute). Top: ascending orbits; bottom, descending orbits.

#### 4.4.4.4.3 flagging the data

Aquarius L3 products are already filtered. No extra-filtering is applied before merging.



## 5 L3 and L4 uncertainty budget

Main CCI products are L4 SSS products estimated at a weekly and a monthly resolution (with a daily and 15days sampling respectively). In these products, uncertainty estimation is performed by using classical least square uncertainty budget. The L2 SSS input random uncertainties are the one presented in the first part of this document for SMOS, SMAP and Aquarius sensors. The relative systematic uncertainties are estimated simultaneously with the monthly SSS L4 estimation. Concerning the SMOS latitudinal systematic uncertainty, it is corrected before the L4 merging. The detailed algorithms are presented in the ATBD v3.

The use of L3 data allows comparing global maps provided for different month and for different orbit types. The project provides specific L3 data, with corrected and uncorrected SSS. These data are used by the validation team which have in charge the product assessment.



## 6 Conclusions and way forward

Phase 1 CCI+ SSS project is dedicated to SMOS-SMAP-AQUARIUS synergy. The merging of different products from different sensors (radiometer for SMAP and AQUARIUS, interferometer for SMOS) shall take into account as input a realistic random and systematic uncertainty model.

The self-consistency between satellite SSS measured by the various sensors and under various geometries have been used for correcting and/or estimating systematic and random uncertainties.

In CCI+SSS phase 1, latitudinal systematic uncertainties have been estimated only for SMOS, assuming that corrections done in other processings will avoid such systematic uncertainties. However this is not the case; in particular systematic seasonal latitudinal uncertainties are observed on Aquarius that could be taken into account following a similar way as the one described here for SMOS.

The characterization of SSS variability remains challenging as, on one hand, the combination of in-situ and satellite information remains to be improved (Stammer et al., 2021); and on the other hand, regions with high SSS variability such as the river plumes or strong surface currents regions are the ones benefiting the most from the satellite information (Tranchant et al., 2019). The statistical distribution of SSS is not expected to be Gaussian (Bingham et al., 2002), especially in regions affected by fresh water inputs, so that vertical, temporal and spatial representativeness uncertainties between in-situ and satellite measurements are not expected to be Gaussian. In particular, the SSS distributions are expected to be skewed towards low SSS values while the higher part of the SSS distributions are expected to vary much less. This lead us to adopt an adjustment of the full time series of CCI L4 SSS and ISAS SSS in fresh and very variable regions based on a high quantile of their statistical distributions. Nevertheless, OI assumption of Gaussian errors might lead to some drawbacks in fresh regions such as river plumes or rainy areas, e.g., an artificial increase (decrease) of the uncertainty during periods with decreased (increased) variability that are very difficult to quantify given the sparseness of existing in-situ measurements. For the reasons outlined above, the estimate and validation of the SSS uncertainty is very tricky and require extended research to go beyond the relatively crude approach presented here.

However, because SSS measurements are contaminated by RFI, a special care has to be done concerning the detection and the RFI removal. So far, we consider the RFI effect as constant in time. But we know that in some cases, RFI present intermittent signature. This means that the systematic uncertainty is not constant in time as we assumed during this phase.

Some uncertainties have not been corrected and could be taken into account during phase 2:



-latitudinal biases for Aquarius and SMAP.

-regional correction by adding a bias correction according to large scale by using climatology or Argo SSS interpolated fields.

-specific uncertainty characterization in Arctic and Antarctic where the ice contamination varies according to the season.

***End of document***